

- 161, Sept. 6, 1968, pp. 1011-1013.
- [3] W. D. Kingery, Ed., *Ice and Snow* (Proceedings of a conference held at the Massachusetts Institute of Technology, Feb. 12-16, 1962). Cambridge, Mass.: M.I.T. Press, 1963.
 - [4] "Bibliography on snow, ice, and permafrost," U. S. Army Cold Regions Res. Eng. Lab., Hanover, N. H., CRREL T. R. 12 (cont. ser.).
 - [5] R. P. Auty and R. H. Cole, "Dielectric properties of ice and solid D₂O," *J. Chem. Phys.*, vol. 20, Aug. 1952, pp. 1309-1314.
 - [6] A. D. Watt and E. L. Maxwell, "Measured electrical properties of snow and glacial ice," *J. Res. Nat. Bur. Stand.* (Radio Propagation), vol. 64D, July-Aug. 1965, pp. 357-363.
 - [7] S. Evans, "Dielectric properties of ice and snow—A review," *J. Glaciol.*, vol. 5, no. 42, pp. 773-792.
 - [8] N. E. Dorsey, *Properties of Ordinary Water Substance in All its Phases: Water-Vapor, Water, and All the Ices*. New York: Reinhold, 1940.
 - [9] Y. Ozawa and D. Kuroiwa, "Dielectric properties of ice, snow, and supercooled water," *Res. Inst. Appl. Elect.*, Hokkaido Univ., monogr. ser., no. 6, 1958, pp. 33-71.
 - [10] S. Ramo, J. R. Whinnery, and T. Van Duzer, *Fields and Waves in Communications Electronics*. New York: Wiley, 1965, chs. 2, 4, 6.
 - [11] J. S. Stratton, *Electromagnetic Theory*. New York: McGraw-Hill, 1941, ch. 1.
 - [12] T. Hatherton, Ed., *Antarctica* (The New Zealand Antarctic Society). Wellington, New Zealand: A. H. and A. W. Reed, 1965, pp. 187-279.
 - [13] A. R. Von Hippel, *Dielectrics and Waves*. New York: Wiley, 1954.
 - [14] C. Montgomery, *Technique of Microwave Measurements* (Radiation Laboratory Series, vol. 11). New York: McGraw-Hill, 1947.
 - [15] T. Yoshino, "The reflection properties of radio waves on the ice cap," *IEEE Trans. Antennas Propagat.*, vol. AP-15, July 1967, pp. 542-551.
 - [16] J. D. Haun and L. W. LeRoy, Eds., *Subsurface Geology in Petroleum Exploration*. Boulder, Colo.: Johnndon, 1958.
 - [17] B. Philbert, "Measurement of permittivity of ice," *J. Glaciol.*, vol. 6, no. 47, 1967, pp. 765-766.
 - [18] J. T. de Bettencourt and J. W. Frazier, "Rock electrical characteristics deduced from depth attenuation rates (in drill holes)," *IEEE Trans. Antennas Propagat.*, vol. AP-11, May 1963, pp. 358-363.
 - [19] R. W. P. King, C. W. Harrison, and D. H. Denton, Jr., "The electrically short antenna as a probe for measuring free electron densities and collision frequencies in an ionized region," *J. Res. Nat. Bur. Stand.* (Radio Propagation), vol. 65D, July-Aug. 1961, pp. 371-384.
 - [20] H. Staras, "The impedance of an electric dipole in a magneto-ionic medium," *IEEE Trans. Antennas Propagat.*, vol. AP-12, Nov. 1964, pp. 695-702.
 - [21] R. C. Carden, T. Laaspere, and B. Pratt, "An experiment to study electric and electromagnetic fields in the frequency range 10 Hz to 540 kHz on OGO-F," *IEEE Trans. Geosci. Electron.*, vol. GE-7, Apr. 1969, pp. 78-88.
 - [22] K. Iizuka, "An experimental study of the insulated dipole antenna immersed in a conducting medium," *IEEE Trans. Antennas Propagat.*, vol. AP-11, Sept. 1963, pp. 518-532.
 - [23] J. Galejs, "Impedance of a finite insulated cylindrical antenna in a cold plasma with a longitudinal magnetic field," *IEEE Trans. Antennas Propagat.*, vol. AP-14, Nov. 1966, pp. 727-736.
 - [24] K. Iizuka and R. W. P. King, "The dipole antenna as a probe for determining the electrical properties of a stratified medium," *IEEE Trans. Antennas Propagat.* (Commun.), vol. AP-10, Nov. 1962, pp. 783-784.

Averaged Pulse-Shape Measurements of Radar Sea Return at Near-Vertical Incidence

NADAV LEVANON, MEMBER, IEEE

Abstract—Some average pulse-shape measurements of radar sea returns at near-vertical incidence are presented. The measurements were made at a 75-cm wavelength, from light aircrafts flying at altitudes of 2 to 2.3 km over various water surfaces.

Greater knowledge of the return shapes could help the design of high-accuracy radar altimeters. It could also contribute to several areas of remote sensing.

Both specular and scattered reflections were observed in all the returns, with clear distinction between the two components. Dominance by either the specular or the scattered component was observed, the first one being the more frequent.

Real-time averaging was obtained by utilizing a sampling technique. This enabled a reduction of the system bandwidth to several hertz, allowing the use of low peak-power RF pulses (1 W), and low-speed chart recorders.

Twenty-one recorded average returns are given, along with an interpretation of the recordings and a description of the measuring system.

Manuscript received November 2, 1970; revised June 4, 1971. This work was supported by NASA under Contract NAS5-11542. The author is with the Department of Environmental Sciences, Tel-Aviv University, Tel-Aviv, Israel.

INTRODUCTION

DESPITE many theoretical and experimental works on radar terrain return, there seems to be no easily available answer to the question: What is the shape of a radar pulse return at near-vertical incidence? Some important works by Moore [1], [2], Edison [3], and Brown [4], give experimental results on earth terrain return, and Evans [5] measured returns from planetary bodies.

The limited number of experimental results is emphasized by the variety of terrains, such as deserts, vegetation, snow, urban areas, lakes, and oceans. It is further emphasized by the variety of states in which each terrain could be found, e.g., wetness of land, roughness of sea, etc.

An answer to this question could contribute to at least two important areas. Firstly, it could help better the design of high-accuracy radar altimeters. Altitude accuracies of the order of 10^{-6} and better are required in

applications such as satellite geodesy [6], oceanography [7], and meteorology. Secondly, it could yield information on some of the terrain characteristics such as roughness, sea state, moisture, etc.

This work presents some measurements of the average shape of radar pulse sea return at a 75-cm wavelength. These were selected from some 700 returns recorded during six flights, over Lake Michigan, Lake Winnebago (Wisconsin), and the eastern Mediterranean near the shore of Israel. Each recorded return is the average (by sampling) of approximately 10^6 received returns. This considerable amount of data partly compensates the limitations of the present system and permits some qualitative interpretation.

The main objective of this paper is to present the recorded shapes of averaged sea near-vertical returns. To the best knowledge of the author such measured waveforms have not been reported before.

Two secondary purposes are 1) to support the view that near-vertical return is a composite of specular and scattered returns and 2) to demonstrate the feasibility of a low-power low-cost return shape measuring system, which utilizes sampling technique for real-time averaging.

SIMPLIFIED THEORETICAL DISCUSSION

In the following discussion, the transmitted pulse is assumed to have a rectangular shape.

Specular Reflection

The specular reflection is a mirror-like coherent reflection in which the shape of the returning pulse is an attenuated version of the transmitted one. As is known from optics, in order to obtain the maximum intensity of the specular component, the mirror should cover the first Fresnel zone. From the height of our flights (2–2.3 km) and the wavelength (75 cm), we get a first Fresnel zone with a diameter of about 60 m. Such a large mirror, that would be perpendicular to the incident radiation, is expected to be found only directly beneath the radar.

Moore and Williams [1] give the following equation for the mean received power:

$$P_R(t) = \frac{P_T G^2(0, \phi) \lambda^2 K}{(4\pi)^2 (2h)^2} \quad (1)$$

where

- $P_R(t)$ mean received power at time t ($t=0$ is the arrival time of the first return);
- P_T transmitted power;
- h altitude;
- $G(0, \phi)$ antenna gain, straight down;
- λ wavelength of the carrier radiation;
- K reflection coefficient, including an indication of what part of the required mirror was actually existing.

For a given geometry and sea state, the mean received power is, therefore, a constant. On a phasor

diagram, this last statement and the coherency assumption cause the vector representing the specular field to be of fixed length and angle.

Scattered Reflection

The scattered reflection is a noncoherent reflection from many scatterers on the surface. The first return is a reflection of the leading edge from the radar subpoint. The illuminated area then grows until the trailing edge is reflected from the subpoint, while the leading edge is reflected from a circle whose radius is approximately $(ch\tau)^{\frac{1}{2}}$, where τ is the length of the transmitted pulse, and c is the velocity of light. At this time, if the antenna beam width is not limiting, the returned power reaches its peak. Moore and Williams [1] have shown that the mean power envelope of the received pulse is a convolution integral of the transmitted pulse with a function representing the effects of the incidence angle on the average scattering cross section $-\sigma^\circ$ of the ocean, the radar antenna pattern, and the additional attenuation due to a longer path toward a side reflection. They have also shown that if the transmitted pulse duration is considerably shorter than the delay, and the antenna pattern and the ground reflection pattern is assumed constant over the participating angles, then the envelope of the leading edge of the return is given by:

$$P_R(t) = \frac{P_T G^2 \sigma^\circ \lambda c t}{4(4\pi)^2 h^3}, \quad 0 < t < \tau. \quad (2)$$

In other words, under these assumptions, the convolution integral is replaced by a regular integral and a transmitted rectangular pulse is reflected back as a linear ramp for the duration of one transmitted pulse. Then, for $t > \tau$, those assumptions become less accurate, and the convolution integral will cause a slow decay of the received signal which constitutes the trailing edge.

The scattered field is a random variable. Most authors assume Rayleigh probability density for the field intensity, and an equal probable phase between $-\pi$ and $+\pi$. Less information is available on the power spectrum in cases of near-vertical return. The power spectrum is partly related to the sea state, the size and geometry of the illuminated area, and the movement of the radar set. Nathanson [8] has accumulated results of several authors on the relation between surface wind velocity and sea clutter bandwidth at low-grazing angles. His summary is that the half-power width of the sea clutter, Δf (Hz), is related to the wind velocity, v (knots), and the wavelength, λ (m), by the linear relation

$$\Delta f = 0.24v/\lambda. \quad (3)$$

At our wavelength (0.75 m) and at wind velocity of 10 knots, Δf will equal 3 Hz. The power-spectrum broadening as a result of the airborne radar set movement could be calculated [2] as a function of the aircraft height and velocity, and $\sigma^\circ(\theta)$. Crude calculations will show that the

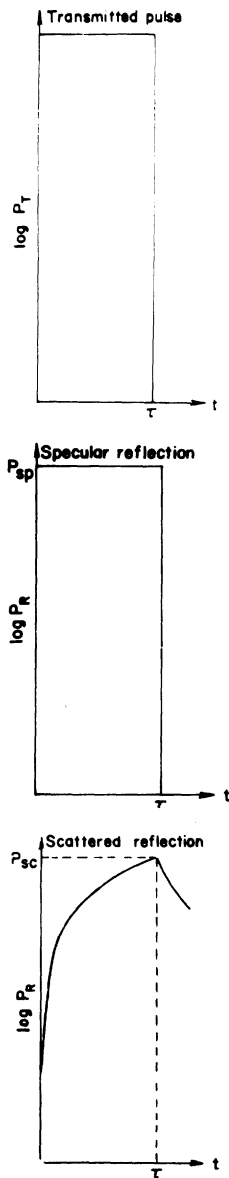


Fig. 1. Specular and scattered theoretical average reflections of a rectangular transmitted pulse.

half-power width due to this contribution will also be in the order of a few hertz. The above discussion leads us to conclude that on the phasor diagram the vector representing the scattered field has a Rayleigh probability density; its mean power increases linearly, its phase is equiprobable between $-\pi$ and $+\pi$, and its power spectrum is a few hertz wide. The last two statements mean that, on the average, the vector will cross any particular angle several times/s.

Composite Reflection

Both the specular and the scattered reflection always exist. However, their proportions change with sea state. The average shape of each one by itself appears in Fig. 1. There, P_{sp} is the constant power of the specular return and P_{sc} is the average power of the scattered reflection at the peak of the envelope, i.e., at $t = \tau$. Note that the logarithmic power scale distorts the linear ramp.

The power envelope of the composite reflection is the sum of the two envelopes. In Fig. 2 four theoretical cases appear, in which the ratio P_{sp}/P_{sc} equals 100, 10, 1, and 0.1, respectively. The logarithmic power scale emphasizes the significant transition in the shape of the return around the ratio $P_{sp}/P_{sc} = 1$.

When $P_{sp} > P_{sc}$, the envelope resembles the rectangular shape of the transmitted pulse. More precisely, it rises from P_{sp} at $t = 0$ to $P_{sp} + P_{sc}$ at $t = \tau$. However, at that moment the envelope does not drop to zero; instead it drops to P_{sc} , and from then on follows the envelope of the scattered reflection.

When $P_{sp} < P_{sc}$, the leading edge becomes more complicated. At $t = 0$ there is a sharp rise to the level P_{sp} . During $0 < t < \tau$ the power rises (linearly) until at $t = \tau$ it reaches the level $P_{sp} + P_{sc}$. The drop at that moment, due to the disappearance of the specular reflection, is less noticed. Again, for $t > \tau$ there remains the long trailing edge of the scattered reflection.

The return envelopes in Fig. 2 do not include fading. They are each the result of averaging many returns during a period much longer than the autocorrelation time constant. For shorter averaging periods fading is noticed. When $t > \tau$ the fading range is that of the scattered reflection. When $t < \tau$ the fading range depends on the relative intensities of the two components. If $P_{sp} > P_{sc}$, the specular component which was assumed to be free of fading predominates the return, and the range of fading is relatively small. Again, the case where $P_{sp} < P_{sc}$ is more complicated. During the rise of the scattered average envelope, there is a moment when the average scattered field equals the specular field (e.g., when $P_{sp} = 0.1 P_{sc}$; this will occur at $t = 0.1 \tau$). On the phasor diagram [9] this situation will be described by the sum of a vector of fixed length and direction, and a vector of the same length (on the average) with random direction, which happens to cross any particular angle several times/s. Clearly, when the two vectors happen to be out of phase, the chances for a large dip in the envelope are relatively high. In other words, the interference between the specular and the scattered fields will cause the fading of the composite return to be larger than the fading range of the scattered field alone. The logarithmic power scale will emphasize the nulls rather than the peaks. The time when such nulls are most likely is given by

$$t_{null} = \tau P_{sp} / P_{sc}. \tag{4}$$

The mathematical justification for the above discussion is given in the Appendix.

THE MEASURING SYSTEM

The measuring system was a modified radio altimeter used for balloon-borne applications [10]. The recording of each complete return usually requires a high bandwidth. Since we are interested in the average return, the system bandwidth could be reduced by applying real-time averaging. This was done by utilizing sampling

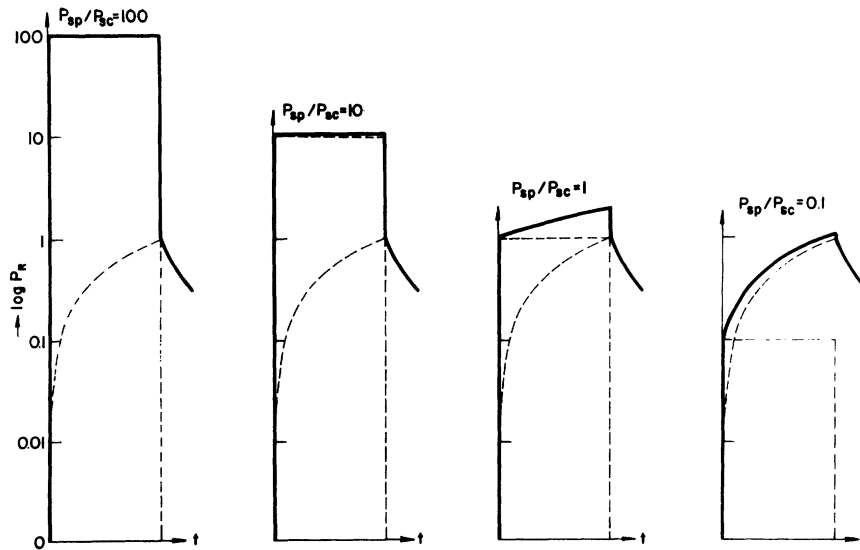


Fig. 2. Composite theoretical returns caused by four different ratios between the specular and the scattered components.

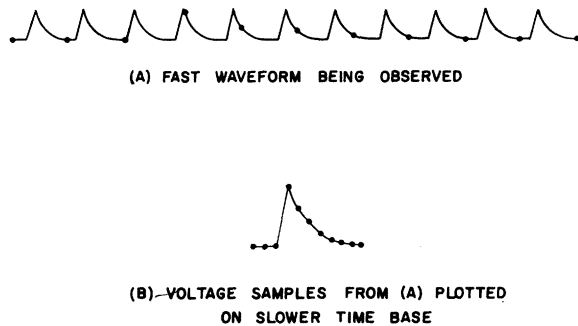


Fig. 3. Principle of sampling technique.

technique. With such a technique there is no need for the complete shape of each single return; rather, each return is sampled once, at a discrete point. Each sample is taken on a different return at progressively later and later points (Fig. 3). These samples reconstruct the shape of the return on a much slower time base, hence a narrower bandwidth.

A simplified block diagram of the system is given in Fig. 4. This is a pulse radar system where the pulse repetition rate is varied by a VCO following a sawtooth function. A receiving window exists before each transmitted pulse. As the pulse period approaches the delay time of the returning pulse, the receiving window samples the return. After the repetition frequency is filtered out, and a correction is inserted to compensate for the increasing density of samples, the output of the receiver is recorded on a chart recorder to yield the shape of the returned pulse.

The transmitter, receiver, and gates and delay blocks of Fig. 4 are all combined in a single superregenerative stage. Such a stage, when quenched into oscillations, shows a receiving sensitivity at the beginning of the oscillations growth, which upon reaching saturation becomes the transmitted pulse. The superregenerative

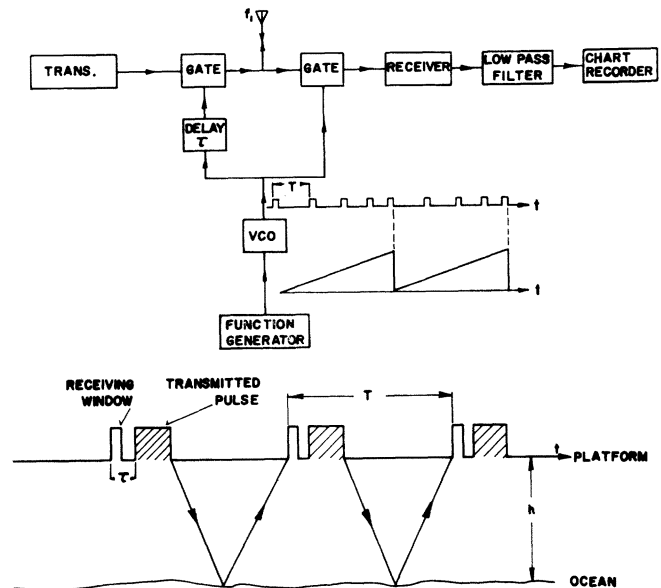


Fig. 4. Measuring system principle of operation and block diagram.

stage is inherently a logarithmic receiver with a wide dynamic range.

Another deviation from the simplified block diagram is a small sinusoidal perturbation superimposed on the linear-voltage ramp fed to the VCO. That perturbation is synchronously detected from the return signal, resulting in the derivative of the shape, rather than in the pulse shape itself. An integrator is then added before the shape is recorded on the chart recorder. This scheme has some advantages, including a 3-dB improvement in signal-to-noise ratio. However, it adds some limitations which will be discussed later. The compensation for the linear increase in sample density is a fixed bias fed to the input of the integrator.

The general system parameters are summarized in Table I. The system is very simple and light. It was

TABLE I
MEASURING SYSTEM PARAMETERS

Altitude	2-2.3 km
Radio frequency	403 MHz
Peak RF power	1 W
Pulsewidth	0.2-0.6 μ s (controlled)
Pulse-repetition frequency	30-100 KHz
Perturbation frequency	200 Hz
Antenna	2 elements Yagi
Polarization	linear
Dynamic range	60 dB
Baseline level (approx.)	-95 dBm
Scanning rate	0.2-0.5 μ s/s (controlled)
Radar system input power	2 W
Radar weight	1 lb

flown on board small aircraft (Cessna 172 and Cherokee 6). If telemetry were used to separate the radar section from the recording section, the first one could be carried aloft by a small meteorological balloon.

THE SYSTEM LIMITATIONS

Several limitations of the system should be mentioned before attempting to analyze the results.

1) Antenna beamwidth and direction—The two element Yagi antenna used in all flights has a relatively wide beam and should start affecting the return significantly only late in the trailing edge. Yet, if the beam is tilted, either because it is misplaced with respect to the aircraft body, or because the aircraft itself tilts, the effect on the return will be twofold, the specular component will be partly attenuated, and the peak of the scattered component will be delayed. A tilt of 15° at an altitude of 2.3 km can cause this delay to be 0.5 μ s.

2) Baseline—The stage prior to the recorder is an integrator. Hence, the baseline is an integral of random noise, and has fluctuations as well as accumulated random dc level. In addition, a fixed bias is fed at the input of the integrator to compensate for the linearly increasing density of samples. If overcompensation or undercompensation occurs, the baseline will have an undesired slope. The baseline position during the return can be deduced from its trend before and after the return.

3) Transmitted pulse—The transmitted pulse is not a perfect rectangle. A typical transmitted pulse has a rise time (10 percent to 90 percent) of 130 ns, and a fall time of 45 ns.

4) Power scale—While the horizontal time scale can be maintained and calibrated accurately, the vertical power scale is only relative, and its accuracy is ± 15 percent. As a crude reference, the absolute level of the baseline is approximately -95 dBm.

5) Harmonic operation—Scanning the delay range is accompanied by an increase in the pulse-repetition frequency, since each receiving window is followed by a transmitted pulse. When this is added to the fact that the delay of the received leading edge is not much longer than the length of the received trailing edge, it becomes

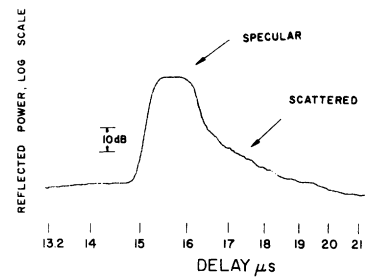


Fig. 5. Recorded sea return (flight 3).

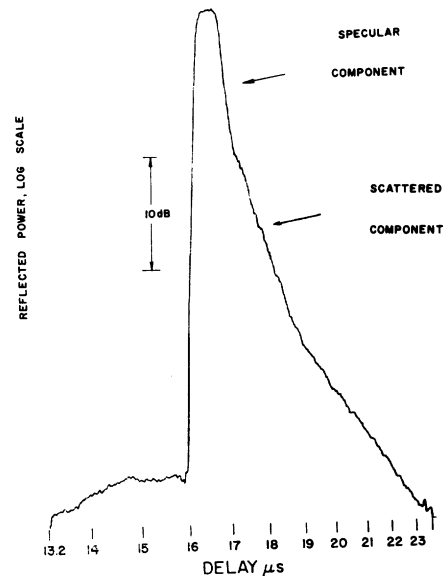


Fig. 6. Recorded sea return (flight 3).

clear that when the receiving window scans the leading edge of the prior pulse reflected from the ocean, it also scans the trailing edge of the reflection of the pulse preceding this prior one.

6) Receiving window width—The width of the receiving window is determined mainly by the amplitude of the sinusoidal perturbation superimposed on the voltage ramp fed to the VCO. It is also affected by the superregenerative stage rate of oscillations growth. The period during the beginning of the oscillations build-up, which is sensitive to the received signal, is not easily defined. However, it is considerably shorter than the chosen perturbation width. Perturbation width could not be reduced without limit. The detected perturbation is the system's actual input signal. Reducing its width would have reduced the signal-to-noise ratio. Calculated on the basis of the perturbation amplitudes, the effective receiving window widths were; 100 ns in flights 1-2 and 20 ns in flights 3-6.

MEASURED RETURNS

Returns recorded during six flights are given in this section. The flight details are summarized in Table II.

Figs. 5 and 6 were both recorded during flight 3. The specular reflection was predominant during this flight,

TABLE II
FLIGHT DETAILS

Flight Number	Date	Local Time	Aircraft	Barometric Altitude (ft)	Flight Path	Sea State	Maximum Wave Height (m)	RF Stage
1	23.10.69	10:30-13:00	Cessna 172	6700	Lake Winnebago	calm	0.1	vacuum tube
2	19.11.69	12:00-15:00	Cessna 172	7200	Lake Michigan off Milwaukee	slight	1.2	vacuum tube
3	28. 6.70	12:00-13:10	Cherokee 6	7400	Mediterranean off Tel-Aviv	smooth	0.5	vacuum tube
4	27. 7.70	10:15-11:30	Cherokee 6	7400	Mediterranean off Tel-Aviv	slight	1.0	vacuum tube
5	17.8.70	10:45-12:10	Cherokee 6	7400	Mediterranean off Tel-Aviv	moderate	1.5	transistor
6	17. 8.70	15:10-16:30	Cherokee 6	7400	Mediterranean off Tel-Aviv	slight	1.2	transistor and vacuum tube

which explains the rectangular shape of the pulse. The transition from specular to scattered reflection, at $t = \tau$, is clearly visible. To remove a possible doubt, the flat top of the pulse could not have been the result of saturation in the measuring system. The dynamic range of the system was wider than the range occupied by the sea return. This was tested in the laboratory with simulated returns. Figs. 7-11 were all recorded during flight 5. During this flight the scattered component was the predominant one. All the returns are characterized by the sharp fading-free rise time of the specular component. It is followed by the logarithmic rise (due to the logarithmic scale) of the scattered component which is more susceptible to fading. The point where the scattered component takes over is preceded, in most cases, by a relatively deep null. This is the null discussed in the theoretical section on composite reflection. In Figs. 7-11, the return peaks appear about $0.5 \mu\text{s}$ later than the theory suggests. This may give rise to the speculation that the antenna beam was tilted during this flight. This speculation is supported by the relatively weak specular component observed in this flight.

Figs. 12-14 are returns recorded during flight 6, which took place several hours after flight 5, over the same path. The instrument used for recording returns 12 to 14 was the same as the one used for returns 7 to 11 (transistorized RF stage). The only differences were a slight change in the antenna position and a calmer sea. This time the specular reflection was dominant. Similar dominance by the specular reflection is observed in Fig. 15, which was also recorded during flight 6, however, with the vacuum-tube RF stage.

Figs. 16 and 17 were recorded during flight 4. Fig. 16 is a sequence of four consecutive sea returns emphasizing the repeatability gained by averaging. Since the baseline during these recordings was not flat, a baseline

recorded in the absence of a return is given for reference. For comparison, a return recorded over the city of Tel-Aviv during the same flight is given in Fig. 17.

Figs. 18 and 19 are returns recorded during flight 2 over Wisconsin. Fig. 18 is a land return recorded several km west of Milwaukee. The specular component is again the dominant one. Fig. 19 is a return from Lake Michigan, several km east of Milwaukee. The vertical scale is the same in both recordings, but the lake return is attenuated by 6 dB. The lake return seems to be dominated by scattered reflection, however the narrow time scale prevents clear distinction.

Figs. 20-23 were recorded during flight 1. The first two were recorded over Lake Winnebago, and the last two are land returns recorded several km south of Fond du Lac, Wisconsin. All four returns are dominated by specular reflection. The land returns differ from the lake returns by their weaker specular component, and by stronger fading of the trailing edge. Lake Winnebago is the smallest water surface from which returns, described in this work, were recorded. This may raise the legitimate doubt of whether the whole return was reflected from the water surface. To remove this doubt, it should be pointed out that Lake Winnebago is 45 km long, and 6 to 16 km wide. From an altitude of 2 km, only echoes arriving $10 \mu\text{s}$ after the leading edge of the received pulse could be contributions from the shore and our time scale did not extend that far. It should be noted that in this flight, and this one only, the time scale is not accurate; its highest value could be off by $2 \mu\text{s}$.

It should also be repeated here that the effective width of the receiving window during flights 1 and 2 was approximately 100 ns, which is five times wider than those during the other flights. This wider window could be partly responsible for the roundness of the returns in Figs. 20-23.

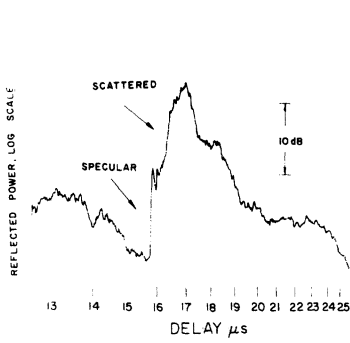


Fig. 7. Recorded sea return (flight 5).

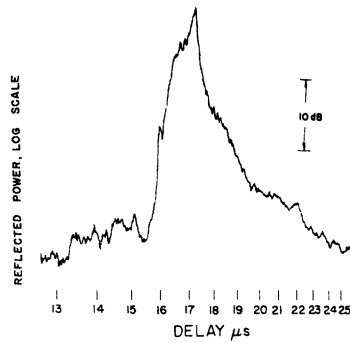


Fig. 8. Recorded sea return (flight 5).

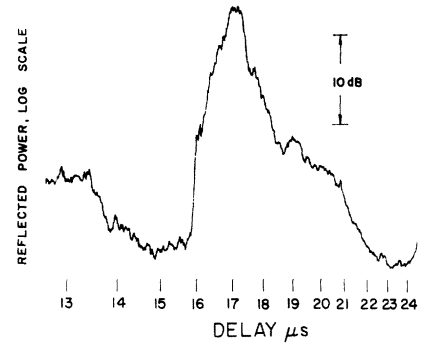


Fig. 9. Recorded sea return (flight 5).

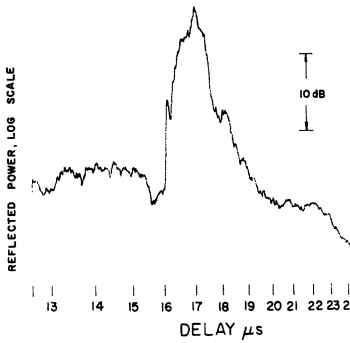


Fig. 10. Recorded sea return (flight 5).

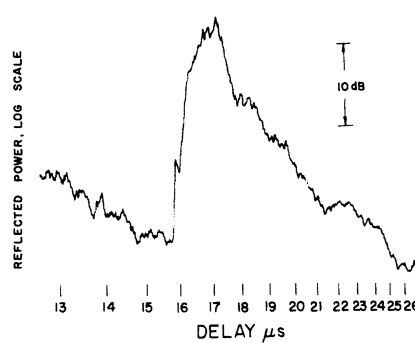


Fig. 11. Recorded sea return (flight 5).

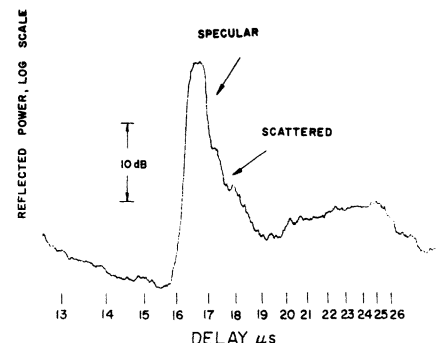


Fig. 12. Recorded sea return (flight 6).

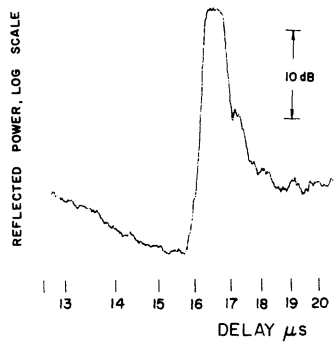


Fig. 13. Recorded sea return (flight 6).

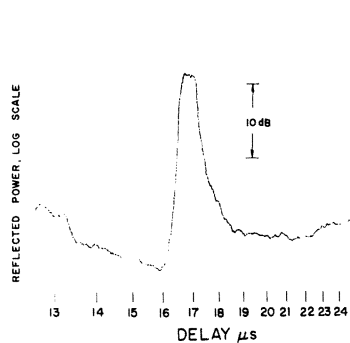


Fig. 14. Recorded sea return (flight 6).

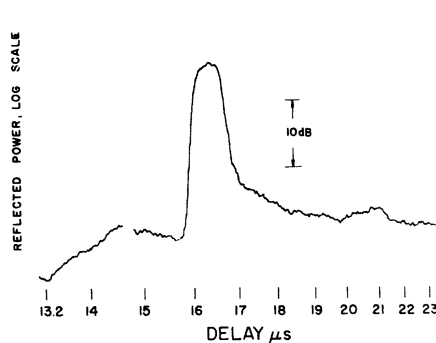


Fig. 15. Recorded sea return (flight 6).

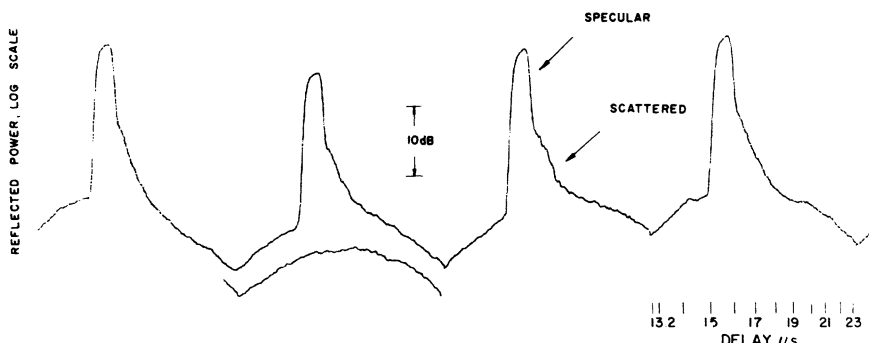


Fig. 16. Sequence of four sea returns with a reference baseline (flight 4).

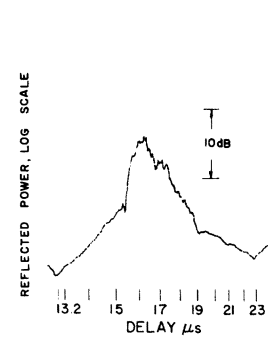


Fig. 17. Return recorded above the city of Tel-Aviv (flight 4).

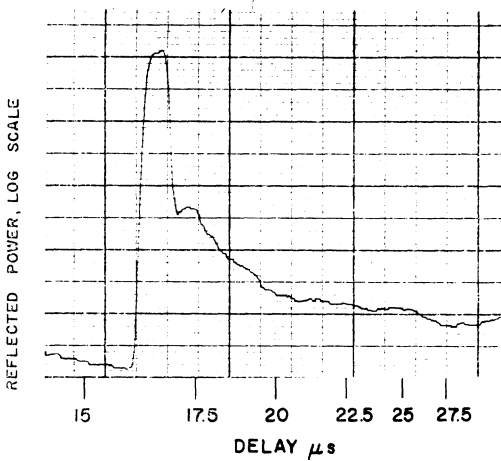


Fig. 18. Recorded land return (flight 2).

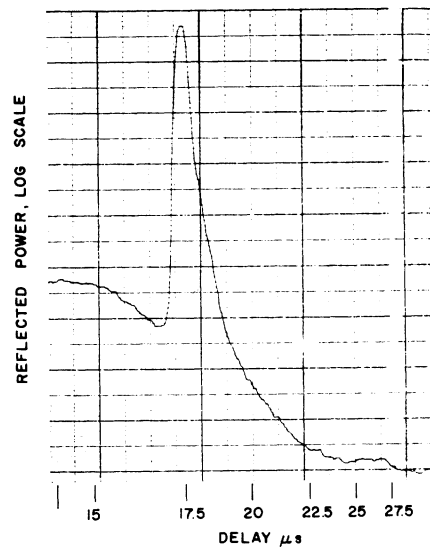


Fig. 19. Recorded lake return (flight 2).

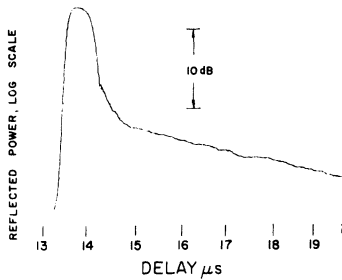


Fig. 20. Recorded lake return (flight 1).

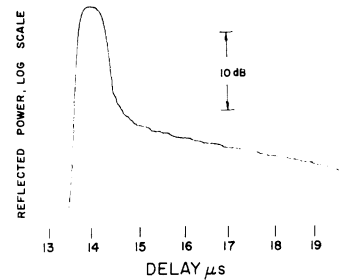


Fig. 21. Recorded lake return (flight 1).

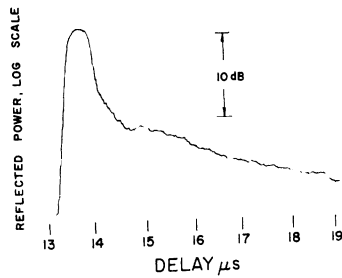


Fig. 22. Recorded land return (flight 1).

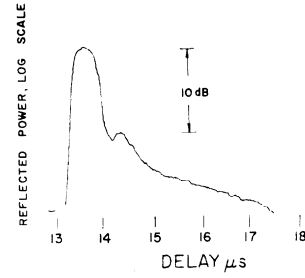


Fig. 23. Recorded land return (flight 1).

SUMMARY AND CONCLUSIONS

The measuring system described here suffers from several limitations. The two most severe ones are the uncertainty in antenna beamwidth and direction and the uncertainty in the recordings' baseline position.

Yet, the results obtained, real-time recordings of average shapes of pulse radar near-vertical returns, are new and interesting and warrant being presented as they are.

Furthermore, the twenty-one recorded waveforms given in this paper are typical representatives of some 700 returns, recorded during six different flights. Each recorded return is the average (by sampling) of approximately 10^6 received returns. This considerable amount

of data partly compensates for the limitations of the present measuring system and justifies some qualitative interpretation.

The presented interpretation is based on the overall shape of the returns, and on sharp transitions, sometimes even accompanied by a notch, between what were referred to as the specular and scattered components. The distinct difference between the two components with respect to amplitude and fading, and the well-defined boundary between them, gives support to the view that the two components are affected by reflections of different characters.

The summarized interpretation is that at a 75-cm wavelength, and from altitudes of 2 to 2.3 km, sea and

lake returns were always a composite of specular and scattered reflections, with a varying proportion between the two components. The ratio of the two determines the overall shape of the returned pulse. Returns dominated by specular reflection were considerably different in shape than those dominated by scattered reflection. In both cases it was always possible to distinguish between the specular and the scattered contribution.

Despite the system limitations, it is believed that the results demonstrate the feasibility of a low-power low-cost return shape measuring system, which utilizes sampling technique for real-time averaging. With some improvements, such systems could be used to extend the measurements to a wider scale of sea state, larger variety of terrain, different altitudes, and shorter wavelengths.

APPENDIX

THE RATIO OF SPECULAR AND SCATTERED FIELDS WHICH IS MOST LIKELY TO YIELD NULLS

The probability density of a Rayleigh-distributed scattered field plus specular field is the same as that of sine wave plus noise [11], and is given as

$$p(v) = \psi^{-1/2} \exp [-(v^2 + a^2)/2\psi] I_0(va/\psi) \quad (5)$$

where

- v envelope field;
- ψ mean square field;
- a sine-wave peak field;
- $I_0(\)$ modified Bessel function.

We are looking for the ratio ψ/a^2 which yields the highest probability of small v . We will find this ratio by requiring

$$\lim_{v \rightarrow 0} \partial p / \partial \psi = 0. \quad (6)$$

The derivative of (5) is

$$\begin{aligned} \partial p / \partial \psi = & [(v^2 + a^2 - \psi)(1/2)I_0(va/\psi) - vaI_1(va/\psi)] \\ & \cdot \psi^{-5/2} \exp [-(v^2 + a^2)/2\psi]. \quad (7) \end{aligned}$$

Using

$$\lim_{x \rightarrow 0} I_0(x) = 1 \quad (8)$$

and

$$\lim_{x \rightarrow 0} I_1(x) = 0 \quad (9)$$

we get

$$\lim_{\psi \rightarrow 0} \partial p / \partial \psi = (a^2 - \psi)(1/2)\psi^{-5/2} \exp (-a^2/2\psi). \quad (10)$$

Equations (6) and (10) will give

$$a^2 = \psi \quad (11)$$

which means that the highest probability for nulls exists when the specular field equals the scattered field.

ACKNOWLEDGMENT

The author wishes to thank Prof. V. E. Suomi and Prof. F. G. Stremmer for their encouragement and help which enabled this work. Thanks go also to C. D. Blair and A. Slonim for their fine work on the instrumentation.

REFERENCES

- [1] R. K. Moore and C. S. Williams, Jr., "Radar terrain return at near-vertical incidence," *Proc. IRE*, vol. 45, Feb. 1957, pp. 228-238.
- [2] R. K. Moore, "Ground echo," in *Radar Handbook*, M. I. Skolnik, Ed. New York: McGraw-Hill, 1970, ch. 25.
- [3] A. R. Edison, R. K. Moore, and B. D. Warner, "Radar terrain return measured at near-vertical incidence," *IRE Trans. Antennas Propagat.*, vol. AP-8, May 1960, pp. 246-254.
- [4] W. E. Brown, Jr., "Radar studies of the Earth," *Proc. IEEE*, vol. 57, Apr. 1969, pp. 612-620.
- [5] J. V. Evans and T. Hagfors, "Study of radio echos from the moon at 23 centimeters wavelength," *J. Geophys. Res.*, vol. 71, Oct. 1966, pp. 4871-4889.
- [6] "Space geodesy altimeter study," Raytheon Company, Final Rep on NASA Contract NASW-1709, Oct. 1968.
- [7] "August study in solid-earth and ocean physics," Rep. to NASA of study at Williamstown, Mass., Aug. 1969.
- [8] F. E. Nathanson, *Radar Design Principles*. New York: McGraw-Hill, 1969, pp. 241-246.
- [9] C. I. Beard, I. Katz, and L. M. Spetner, "Phenomenological vector model of microwave reflection from the ocean," *IRE Trans. Antennas Propagat.*, vol. AP-4, Apr. 1956, pp. 162-167.
- [10] N. Levanon, "Balloon-borne radio altimeter," *IEEE Trans. Geosci. Electron.*, vol. GE-8, Jan. 1970, pp. 19-30.
- [11] S. O. Rice, "Mathematical analysis of random noise," *Bell Syst. Tech. J.*, vol. 23, 1944, pp. 282-332, and vol. 24, 1945, pp. 46-156.